HHS Public Access

Author manuscript

ACS Appl Mater Interfaces. Author manuscript; available in PMC 2019 October 03.

Published in final edited form as:

ACS Appl Mater Interfaces. 2018 October 03; 10(39): 33088–33096. doi:10.1021/acsami.8b13571.

Cardiac Stem Cell Patch Integrated with Microengineered Blood Vessels Promotes Cardiomyocyte Proliferation and Neovascularization after Acute Myocardial Infarction

Teng Su[†,‡,#], **Ke Huang**[†,‡,#], **Michael A. Daniele**[†,§,#], **Michael Taylor Hensley**[†,‡], **Ashlyn T. Young**[†], **Junnan Tang**[‡,‖], **Tyler A. Allen**[†,‡], **Adam C. Vandergriff**[†,‡], **Patrick D. Erb**[†], **Frances S. Ligler**[†], and **Ke Cheng**[*,†,‡,⊥]

[†]Joint Department of Biomedical Engineering, University of North Carolina at Chapel Hill and North Carolina State University, Raleigh, North Carolina 27695, United States

[‡] Department of Molecular Biomedical Sciences and Comparative Medicine Institute, North Carolina State University, 1060 William Moore Drive, Raleigh, North Carolina 27607, United States

[§] Department of Electrical and Computer Engineering, North Carolina State University, Raleigh, North Carolina 27695, United States

[‖]Department of Cardiology, The First Affiliated Hospital of Zhengzhou University, Zhengzhou, Henan 450052, China

[⊥]Divison of Pharmacoengineering and Molecular Pharmaceutics, Eshelman School of Pharmacy, University of North Carolina at Chapel Hill, Chapel Hill, North Carolina 27599, United States

Abstract

Cardiac stem cell (CSC) therapy has shown preclinical and clinical evidence for ischemic heart repair but is limited by low cellular engraftment and survival after transplantation. Previous versions of the cardiac patch strategy improve stem cell engraftment and encourage repair of cardiac tissue. However, cardiac patches that can enhance cardiomyogenesis and angiogenesis at the injured site remain elusive. Therapies that target cardiomyocyte proliferation and new blood vessel formation hold great potential for the protection against acute myocardial infarction (MI). Here, we report a new strategy for creating a vascularized cardiac patch in a facile and modular fashion by leveraging microfluidic hydrodynamic focusing to construct the biomimetic microvessels (BMVs) that include human umbilical vein endothelial cells (HUVECs) lining the luminal surface and then encapsulating the BMVs in a fibrin gel spiked with human CSCs. We

[*]**Corresponding Author:** ke_cheng@unc.edu, ke_cheng@ncsu.edu. Phone: 919 513 6157. Fax: 919 513 7301.

[#]Author Contributions

T.S., K.H., and M.A.D contributed equally to this work. T.S., M.A.D., K.C., and F.S.L. conceived and designed the study; T.S., K.H., M.A.D., M.T.H., A.T.Y., J.T., T.A.A., A.C.V., and P.D.E. performed all the experiments and collected data; T.S., K.H., M.A.D., K.C., and F.S.L. wrote the paper with input from all authors who reviewed and approved the final submission.

Supporting Information

The Supporting Information is available free of charge on the ACS Publications website at DOI: 10.1021/acsami.8b13571. Detailed procedures of cell isolation and culture; microfabrication of BMVs; cell viability and proliferation in BMVs; immunofluorescent studies of BMVs; and morphological and rheological analyses of cardiac patches (PDF)

The authors declare no competing financial interest.

show that the endothelialized BMVs mimicked the natural architecture and function of capillaries and that the resultant vascularized cardiac patch (BMV–CSC patch) exhibited equivalent release of paracrine factors compared to those of coculture of genuine human CSCs and HUVECs after 7 days of in vitro culture. In a rat model of acute MI, the BMV–CSC patch therapy induced profound mitotic activities of cardiomyocytes in the peri-infarct region 4 weeks post-treatment. A significant increase in myocardial capillary density was noted in the infarcted hearts that received BMV–CSC patch treatment compared to the infarcted hearts treated with conventional CSC patches. The striking therapeutic benefits and the fast and facile fabrication of the BMV–CSC patch make it promising for practical applications. Our findings suggest that the BMV–CSC patch strategy may open up new possibilities for the treatment of ischemic heart injury.

Graphical Abstract

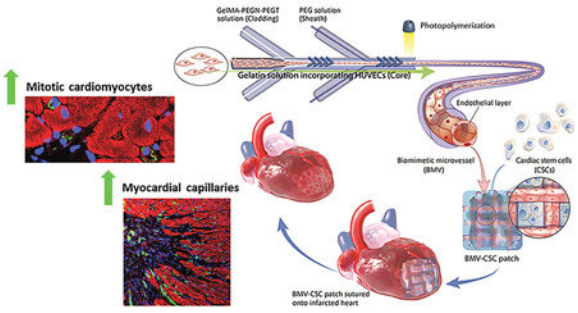

Keywords

microvessels; hydrodynamic focusing; cardiac stem cells; cardiomyocyte proliferation; angiogenesis; myocardial infarction

INTRODUCTION

A fundamental issue with the treatment of myocardial infarction (MI) lies in the minimal capacity of the heart to regenerate following an initial insult.[1] The myocardium is a unique type of tissue that provides persistent contractile force in a highly regulated manner to pump blood efficiently through the body. To support normal function, the tissue requires comprehensive vascular support to satisfy high metabolic demand. Mi-induced ischemia can lead to massive loss of cardiomyocytes and formation of scar tissue that permanently reduces heart function, often leading to heart failure which affects over 40 million people globally and is the leading cause of hospitalizations in the United States.[2] Vascularization is essential to enhance cardiomyocyte survival and heart function.[3] Stem cell therapy represents a promising approach to MI treatment. However, low retention and survival of stem cells in the ischemic myocardium after injection remains a major obstacle limiting the efficacy of cell-based therapy.[4] Previous versions of the cardiac patch strategy improve stem cell retention and promote repair of heart tissue after MI.[5,6] An unmet challenge is to develop a cardiac patch that can promote cardiomyogenesis and angiogenesis at the injured site after implantation.[7]

In the past few years, interest in the design and fabrication of vascularized tissue constructs has increased. Many of those strategies have focused on the seeding of vessel-forming cells into natural or synthetic scaffolds,[8] generation of cellular spheroids or sheets,[9] and implantation of the isolated microvascular fragment,[10] yielding promising results including enhanced blood vessel growth, blood perfusion, and cellular activity of the tissue constructs in vivo. Nevertheless, these approaches rely on the natural process of angiogenesis, which can take weeks to months to happen. Advances in the development of microfabrication technologies allow us to generate highly organized microvascular networks. Microfluidics combined with three-dimensional (3D) printing has been actively investigated to generate delicately organized microchannels to guide the formation of microvasculature in tissue constructs.[11] Recently, we have shown that hydrodynamic focusing is a benign and highly efficient method for fabricating freestanding engineered microvessels capable of accommodating multiple vascular cell types, sprouting, and initiating vascularization.[12–14] The unique properties of these engineered microvessels make them particularly attractive for cardiovascular tissue engineering.

Here, we report a new strategy of creating a vascularized cardiac stem cell (CSC) patch combining stem cells with engineered microvasculature. We fabricated a well-defined biomimetic microvessel (BMV) including human umbilical vein endothelial cells (HUVECs) lining the luminal surface via microfluidic hydrodynamic focusing (Figure 1A). The endo-thelialized BMVs mimic the natural architecture and function of capillaries and venules. Our previous studies have shown that cardiosphere-derived CSCs are safe and effective in early phases of clinical trials for the treatment of MI through a paracrine signaling mechanism.[15,16] Inspired by these studies, we created a vascularized CSC patch (BMV–CSC patch) by integrating the BMVs with human CSCs spiked in a fibrin gel. We hypothesize that (1) the BMVs serve as the transport channels that help the CSCs in the patch obtain nutrients from the surrounding tissue and (2) the endothelium of BMVs induces angiogenesis in the ischemic area. The BMV–CSC patch can engraft on the epicardial surface of the infarcted left ventricle and release stem cell factors to the scarred myocardium after MI. By transplantation of the BMV–CSC patch in an immunodeficient nude rat acute infarct model, we show that the BMV–CSC patch therapy promotes cardiomyocyte proliferation after MI. Moreover, the BMV–CSC patch-induced cardiomyocyte proliferation is accompanied by an enhanced blood vessel formation in the peri-infarct region as well as at the host–patch interface compared with conventional CSC patch treatments. Our work provides a novel facile strategy for the design and development of vascularized CSC patch through integration of engineered blood vessels to promote cardiomyocyte proliferation and neovascularization after ischemic injury.

EXPERIMENTAL SECTION

Cell Isolation and Culture.

Human CSCs were derived from transplantation disqualified donor hearts obtained from Organ Procurement Organization according to previously published methods.[15] The detailed isolation procedure employed in this study is described in the Supporting Information. All procedures were approved by the institutional review board, and written informed consent

was obtained from all patients. The CSCs were used at passages 2–4. Primary HUVECs were obtained from American Type Culture Collection (ATCC). The cells were expanded in the HUVEC growth media consisting ofa vascular cell basal medium (ATCC PCS-100–030) supplemented with endothelial cell growth kit (ATCC PCS-100–041) and used at passages 4–6.

Microfluidic Fabrication of BMVs.

To fabricate the BMVs with HUVECs lining the luminal surface, we utilized a microfluidic device consisting of a central microchannel having two shaping regions. Each shaping region is patterned with a set of four chevron-shaped grooves in the channel walls. The HUVECs comprising the lumen were suspended at a density of 3×10^7 cells·mL^{-1} in 1 wt % gelatin (from porcine skin, Sigma-Aldrich) dissolved in HUVEC growth media to form the core solution. For the cladding solution, gelatin methacrylamide (GelMA) was synthesized as previously described[14] and then mixed with four-arm poly(ethylene glycol) (PEG)-tetra-norbornene (PEGN; 10 kDa, Sigma-Aldrich) and PEG-tetra-thiol (PEGT; 10 kDa, Sigma-Aldrich) at a weight ratio of 2:1:1 in phosphate-buffered saline (PBS). Fibronectin was added at 50 μg·mL^{-} to supplement the GelMA–PEG mixture for further supporting cellular attachment. The outer sheath stream was made of 6 wt % PEG suspended in PBS. Hydrodynamic focusing in microfluidic channels was used to direct these three solutions into coaxial flow patterns. The BMVs were generated by photopolymerization and maintained in HUVEC growth media at 37°C in 5% CO_2. The detailed characterization of the BMVs, including the HUVEC viability and proliferation on the luminal surface, immunofluorescent studies, and morphological analysis are described in the Supporting Information.

Fabrication of Cardiac Patches.

To fabricate the BMV–CSC patch, the BMVs after being cultured for 17 days were arranged biaxially on the bottom surface of one well of a 12-well plate. The Tisseel fibrin gel kit (Baxter) was used to encapsulate both the BMVs and the human CSCs. The final composition of the fibrin gel consisted of 37 mg·mL^{-1} of fibrinogen, 8.0×10^6 human CSCs per mL, 217 U·mL^{-1} of thrombin, and 1270 U·mL^{-1} of aprotinin. The fibrin gel was incubated at 37°C in 5% CO_2 for 15 min to allow complete polymerization before the addition of a 1:1 combination of HUVEC growth medium and CSC growth medium. The as-prepared fibrin gel disk was cut into square pieces (5 mm × 5 mm × 1 mm). Therefore, there were a total of six biaxially aligned 5 mm long BMVs in each patch. For the fabrication of the HUVEC–CSC patch, the fibrin gel solution containing 37 mg· mL^{-1} of fibrinogen, 3.96×10^6 HUVECs per mL, 8.0×10^6 human CSCs per mL, 217 U·mL^{-1} of thrombin, 1270 U·mL^{-1} of aprotinin, and Iscove's modified Dulbecco's media (IMDM) was ejected into one well of a 12-well plate. The as-prepared gel disk was cut into square pieces (5 mm × 5 mm × 1 mm) to give the HUVEC–CSC patches. The CSC patch was fabricated in the same manner but without the addition of HUVECs. The native fibrin gel patch was designated as empty patch. All the patches were maintained at 37°C in 5% CO_2 and fed every day for 8 days prior to transplantation.

In Vitro Release of Paracrine Factors.

The freshly prepared BMV–CSC patches were employed for the release studies. Each patch contained approximately 1.2×10^5 HUVECs and 2.0×10^5 human CSCs. The patches were cultured for 8 days, followed by incubation with 1 mL of serum-free IMDM. For comparison, 1.2×10^5 HUVECs and 2.0×10^5 human CSCs or 1.2×10^5 HUVECs were seeded in one well of a 24-well plate and cocultured for 8 days with daily media change prior to incubation with 1 mL of serum-free IMDM. To investigate the sustained release of paracrine factors, the conditioned media were collected at various time points (days 3, 7, 11, and 14). The concentrations of vascular endothelial growth factor (VEGF) and hepatocyte growth factor (HGF) in the conditioned media were measured using ELISA kits (R&D Systems) according to the manufacturer's instructions. The data were averaged from three independent measurements.

Transplantation of Cardiac Patches into an Athymic Nude Rat MI Model.

All animal work was compliant with the Institutional Animal Care and Use Committee at North Carolina State University (IACUC number: 16–217). As the cardiac patches tested in this study consisted of human cells and a human fibrin gel, we employed nude rats to minimize host immune rejection in animals after patch transplantation. Briefly, 31 female nude rats (5–7 weeks old; Charles River Laboratories) were anesthetized by inhalation of 3% isoflurane in 100% oxygen at a flow rate of 2 $L \cdot min^{-1}$. Under sterile condition, the heart was exposed by a left thoracotomy and acute MI was achieved by permanent ligation of the left anterior descending artery (LAD). Immediately after MI induction, the hearts were randomized to receive one of the following six treatments: (1) Sham group: left thoracotomy without LAD ligation ($n = 4$); (2) MI-only group: left thoracotomy with LAD ligation ($n = 3$); (3) empty patch group: suturing the empty patch onto the infarct surface immediately after MI induction ($n = 6$); (4) CSC group: suturing the CSC patch onto the infarct surface immediately after MI induction ($n = 6$); (5) HUVEC–CSC group: suturing the HUVEC–CSC patch onto the infarct surface immediately after MI induction ($n = 6$); and (6) BMV–CSC group: suturing the BMV–CSC patch onto the infarct surface immediately after MI induction ($n = 6$).

Immunohistochemistry Assessment.

Heart cryosections were fixed with 4% paraformaldehyde in PBS for 30 min, permeabilized and blocked with protein block solution (DAKO) containing 0.1% saponin (Sigma-Aldrich) for 1 h at room temperature. For immunostaining, the samples were incubated overnight at 4°C with the following primary antibodies diluted in the blocking solution: mouse anti-rat sarcomeric α-actinin (α-SA, 1:200, ab9465, Abcam) was used to identify cardiomyocytes; rabbit anti-rat Ki67 antibody (1:200, ab15580, Abcam), rabbit anti-rat histone H3 phosphorylated at serine 10 (pH3, 1:200, ab5176, Abcam), and rabbit anti-rat Aurora B kinase (AURKB, 1:200, ab2254, Abcam) antibodies were used to analyze cell-cycle re-entry, karyokinesis, and cytokinesis, respectively; rabbit antirat/human von Willebrand Factor (vWF, 1:200, ab6994, Abcam) antibody was used to detect myocardial capillaries in the peri-infarct regions; rabbit anti-rat red blood cell (RBC) (1:50, 112–4139, Rockland) and mouse anti-human vWF (1:200, ab201336, Abcam) antibodies were used to analyze the

inoculation of perfused human BMVs with host vessels. After three 10 min washes with PBS, samples were stained for 1.5 h at room temperature with fluorescent secondary antibodies including goat anti-mouse IgG Alexa Fluor 594 conjugate (1:400, ab150116, Abcam), donkey anti-rabbit IgG Alexa Fluor 488 conjugate (1:400, ab150073, Abcam), donkey anti-rabbit IgG Alexa Fluor 555 conjugate (1:400, ab150074, Abcam), and goat anti-mouse IgG–Cy5 conjugate (1:400, ab6563, Abcam) based on the isotopes of the primary antibodies. This was followed by 10 min of 4,6-diamidino-2-phenylindole dihydrochloride (DAPI) staining for nucleus visualization. Slides were mounted with ProLong Gold mountant (Thermo Fisher Scientific) and viewed under a Zeiss LSM 710 confocal microscope (Carl Zeiss). Images were analyzed using NIH ImageJ software.

Statistics.

All experiments were performed independently at least three times, and the results were presented as mean ± standard deviation (SD). Comparisons between any two groups were performed using two-tailed unpaired Student's *t*-test. Comparisons among more than two groups were performed using one-way analysis of variance (ANOVA), followed by post hoc Bonferroni test. Single, double, and triple asterisks represent $p < 0.05$, 0.01, and 0.001, respectively; $p < 0.05$ was considered statistically significant.

RESULTS AND DISCUSSION

BMVs Support HUVEC Attachment, Proliferation, and Maturation.

For decades, there has been a growing need for alternatives to autologous blood vessel grafts for tissue repair. Since the seminal work of Weinberg and Bell,[17] much attention has been given to the construction of tissue-engineered blood vessels (inner diameter > 1 mm) for arterial regeneration.[18] It still remains a challenge to create freestanding functional microvessels that emulate the architecture and function of the microvasculature. Hydrodynamic focusing enables the generation of freestanding microvessels with their size and shape being finely tuned by manipulating the flow-rate ratios of the infused fluids and the number of shaping features in a wide range.[12–14,19] In this study, inspired by the architecture of capillaries and venules, we employed hydrodynamic focusing to surround a continuous flow of suspended HUVECs within a tubular hydrogel shell for the microfabrication of BMV populated with HUVECs on the luminal surface. The hydrogel shell consisted of an interpenetrating network of GelMA and PEG. The covalently cross-linked PEG network was formed by thiol-ene coupling between PEGT and PEGN, whereas the GelMA network was integrated using a concurrent chain-growth polymerization to form a mechanically robust network capable of supporting cell adherence.[13,14]

We utilized a microfluidic hydrodynamic focusing device consisting of two sets of four chevron-shaped grooves in a central microchannel to construct uniform endothelialized microvessels over 1 m in length within 10 min. The BMVs had the inner and outer diameters of 269 ± 15 and 568 ± 7 μm, respectively. The dimensions of BMVs were at the upper end of the size range of mammalian microvasculature whose inner diameter ranges from 2 to 300 μm and outer diameter from 13 to 500 μm.[20,21] Cellular attachment and spreading onto the luminal surface of BMVs were seen after 1 day. After 14 days of culture, a confluent

monolayer of HUVECs lined the luminal surface, mimicking the endothelium of natural blood vessels (Figures 1B and S1). Viability assay using LIVE/DEAD staining revealed that 84.9% of HUVECs remained viable in the BMVs 1 day after seeding. The cell viability significantly increased from day 1 to day 14 and was maintained at over 95% up to 28 days (Figure 1C,D). The proliferation of HUVECs in BMVs was measured as a time-dependent increase in cell density up to 14 days. However, no significant change in cell density was observed between day 14 and day 28 (Figure 1E).

The adherent HUVECs were densely packed on the luminal surface of BMV by day 14, displaying a predominant orientation along the longitudinal axis of microvessel lumen (Figure 1F). Interestingly, the formation of pseudopodia, protrusions, and even capillary-like hollow structures was observed, indicating the maturation of HUVECs in the BMVs (Figure 1G–1).

We investigated the ultrastructure of BMVs, revealing that the interconnected micropores occur ubiquitously in our BMV (Figure 2A) with nanofibrous architecture in the pore wall (Figure 2B). The diameter of the nanofibers ranged from 20 to 50 nm, which is similar to that of the natural collagen IV nanofibrils in the lamina densa membrane layer of the vascular basement membrane.[22] It has been reported that the nano-fibrous architecture of collagen in the extracellular matrix of mammalian tissues is important to cellular behavior (adhesion, proliferation, and differentiation).[23–26] Our BMVs can mimic this nanostructured architecture, which is attractive for their practical applications in tissue engineering.

We further investigated the cellular function in the BMVs. During the period from day 7 to day 14, the cellular expression of tight junction protein (ZO-1) in HUVECs was significantly increased, accompanied by the almost complete disappearance of cycling cells (Figure 3). These results suggested that a confluent layer of endothelial cells lined the BMVs, and the cells underwent contact inhibition to avoid overproliferation in less than 2 weeks, which was consistent with the previous proliferation assay. Therefore, our BMVs provide a proper microenvironment that supports cell growth and regulates endothelial cell–cell interaction. It is worth noting that we only included fibronectin, a component of the extracellular matrix of the blood vessel, into the BMVs for improving cellular adhesion and proliferation. Other basement membrane proteins, including collagen IV, elastin, and laminin, could also be incorporated into the BMVs in a similar fashion to better mimic the in vivo blood vessel microenvironment.

Engineering and Characterization of the BMV–CSC Patch.

The current strategies of fabricating vascularized cardiac patches, including the seeding of vessel-forming cells into natural or synthetic scaffolds, generation of cellular spheroids or sheets, and implantation of the isolated microvascular fragments, are relatively cumbersome. Unlike previous strategies, we utilized the preorganized endothelialized BMVs that allow the facile fabrication of the vascularized CSC patch (termed BMV–CSC patch) in a modular fashion and are amenable to the fabrication of larger-scale patches. To fabricate the BMV–CSC patches, the BMVs after 17 days of culture were embedded with human CSCs into a fibrin gel. The identity of these CSCs was previously characterized by flow cytometry on common CSC markers, indicating that these cells are positive for CD105 and CD90, low for

c-kit, and negative for CD45 and CD34.[15] Transplantation-ready BMV–CSC patches were obtained by cutting the fibrin gel into square pieces (5 mm × 5 mm × 1 mm). To verify that the human CSCs remain viable in the patch, we cultured the BMV–CSC patches in vitro for 22 days. The confluent HUVECs were aligned along the lumen of BMVs, whereas the CSCs were adjacent to the BMVs and well distributed in the microporous structure of the BMV–CSC patch (Figures 4A,B, S2, and S3).

Previous studies indicated that the CSCs exert their therapeutic benefits mainly through paracrine effects, that is, secreted factors from the CSCs promote cardiac regeneration and inhibit fibrosis and inflammation rather than direct differentiation.[15,16] We found that the cells encapsulated within the BMV–CSC patch began to secrete regenerative growth factors during in vitro culture. Enzyme-linked immunosorbent assay revealed that the BMV–CSC patch continuously released pro-myogenic and pro-angiogenic paracrine factors, such as VEGF and HGF, for at least 14 days (Figures 4C,D and S4). It is well-known that VEGF is proangiogenic and HGF promotes cell proliferation, motility, morphogenesis, and angiogenesis and provides tissue protection after injury.[6] The amounts of growth factors released from the BMV–CSC patch were less than those from the CSCs cocultured with HUVECs on the tissue culture plate (TCP) within the first 3 days, possibly because the diffusion of proteins could be retarded by the fibrin matrix in the early stage.[27] After 7 days, the growth factor releases from the BMV–CSC patch were similar to those from the cells cocultured on TCP. The equivalent release of the selected paracrine factors from the 3D patch compared to two-dimensional cultures on plastic was probably facilitated by the swelling of the microporous BMV–CSC patch during in vitro culture. The incorporation of biaxially aligned BMVs enhanced the storage modulus of the fibrin gel patch from 3.9 ± 0.6 to 8.4 ± 1.3 kPa (Figure S5) so that it was closer to that of the rodent myocardium (10–20 kPa) and more compatible for the integration of BMV–CSC patch with host myocardium after implantation.[28]

BMV–CSC Patch Therapy Improves Cardiomyocyte Proliferation in Vivo.

To investigate the potency of the BMV–CSC patch for the treatment of heart injury after MI, we employed an immunodeficient nude rat model of MI created by LAD ligation (Figures 5A and S6). We included three control cardiac patch groups with sizes identical to that of the BMV–CSC patches: (1) patches containing randomly distributed HUVECs and human CSCs (HUVEC–CSC patch); (2) patches containing human CSCs alone (CSC patch); and (3) patches without cells (empty patch). All patches were implanted immediately after LAD ligation. Rat hearts after MI induction or sham operation served as negative or positive controls, respectively.

After implantation for 4 weeks, all patches could be identified by their appearance and location, covering all or a portion of the infarcted myocardium. It has established that adult cardiomyocytes have extremely limited capacity to proliferate in vivo. We first assessed the cardiomyocyte cell-cycle activity 4 weeks after the patch implantation by α-sarcomeric actinin (α-SA) and Ki67 expressions (Figures 5B and S7). Figure 5B shows that few Ki67-positive cardiomyocytes appear in the hearts treated with empty patch, whereas a number of proliferating noncardiomyocytes (Ki67-positive but negative for α-SA) are evident. The

CSC patch treatment seemed to encourage the cardiomyocyte cell-cycle re-entry, which is consistent with the previously reported therapeutic effects of CSCs.[15,16] The HUVEC–CSC patch treatment increased the proliferating cardiomyocytes in the infarcted myocardium. Notably, a larger number of cycling cardiomyocytes were found in the peri-infarct region of the BMV–CSC patch recipient hearts compared with those of the CSC patch and HUVEC–CSC patch recipients (Figure 5C).

We further stained the patch-recipient heart sections for a specific marker of late G2/mitosis, pH3, and a marker of cytokinesis, AURKB (Figures 6A,C and S8). Remarkably, our BMV–CSC patch induced the robust mitotic activity of cardiomyocytes in the injured hearts after 4 weeks of treatment as evidenced by the elevated number of pH3-positive as well as AURKB-positive cardiomyocytes at the peri-infarct zone compared to other patch treatments (Figure 6B,D). Expression of AURKB suggested that the cardiomyocytes not only entered the cell cycle but also were undergoing cytokinesis (Figure 6C). In addition, the proliferating cardiomyocytes did not express human nuclear antigen, indicating that these cells were of endogenous origin, not originated from the human CSCs in the patch (Figure S9). Taken together, these results indicate that the BMV–CSC patch therapy can induce significant mitotic activities of cardiomyocytes in the peri-infarct region after MI.

BMV–CSC Patch Therapy Enhances Neovascularization in Vivo.

We further evaluated whether vascular growth was coincident to cardiomyogenesis. The BMV–CSC patch recipient hearts showed the remarkably higher number of vWF-positive vasculatures in the peri-infarct region compared with other patch recipient hearts (Figures 7A,B and S10). Sections stained for rat RBCs confirmed perfusion of the human vessel lumen with rat RBCs in the BMV–CSC patch-recipient hearts (Figure 7C), suggesting the anastomosis of patch microvessels with the host vasculature. In addition, we investigated the angiogenesis occurring near the host-patch interface in the hearts treated with CSC patches, HUVEC–CSC patches, and BMV–CSC patches, respectively. Tissues underneath the HUVEC–CSC and CSC patches were primarily fibrotic. Excitingly, sizable endomyocardium was preserved underneath the BMV–CSC patches. Repeated examples of vWF-positive capillaries at the host-patch interface of the BMV–CSC patch-treated heart were also visible (Figure 7D). Together, these results suggested that the BMV–CSC patch treatment promotes endogenous cardiomyocyte proliferation, which is accompanied by the enhanced vascular growth in the post-MI heart. This is possibly due to the BMV–CSC patch that could exert its therapeutic benefits not only through enhancing the paracrine effects of CSCs and activating the angiogenic and myogenic signaling in the peri-infarct region but also through the integration of BMVs with the host vasculature.

CONCLUSIONS

The innovation of our BMV–CSC patch strategy is as follows: (i) unlike previous studies incorporating randomly distributed endothelial cells or endothelial progenitor cells in the patch,[3,8] the present study utilizes the preorganized endothelialized BMVs that allow the facile fabrication of vascularized cardiac patches and are amenable to the fabrication of larger-scale patches. (ii) The BMVs are further embedded in a biological scaffold spiked

with CSC s to create a “vessel-in-parenchyma” construct. When the BMV–CSC patch is transplanted onto the acutely infarcted myocardium, this structure maybe beneficial in helping the CSCs in the patch get nutrients from the heart so as to facilitate their survival in the challenging infarct environment. Furthermore, it has been suggested that intimate interactions exist between the cardiac vasculature and CSCs.[29] The BMVs may also contribute to a protective microenvironment for CSCs, with a reciprocal impact on the CSC-induced angiogenic signaling in infarct healing.[30,31] Therefore, the BMV–CSC patch treatment exhibits enhanced therapeutic efficacy compared to the HUVEC–CSC patch and CSC patch treatments. It is worth noting that in this study, the BMV–CSC patch was delivered through open-heart surgery. In the future, minimally invasive approaches can be explored to place the patch on the heart surface. The present study was also limited by the acute infarct model used, small sample size, and 4-week endpoint. For clinical applicability, a large animal model of MI and longer study duration will be needed to fully characterize the efficacy and safety of the BMV–CSC patch. The investigation of therapeutic benefits of BMV–CSC patch treatment in a porcine model of acute MI is currently underway.

In summary, we report a vascularized BMV–CSC patch to promote cardiomyocyte proliferation and neovascularization after acute MI. Although our current study targets the heart, the hydrodynamic focusing technology for making BMVs can be adapted to design other BMVs that emulate native vasculature. By fine-tuning the physicochemical parameters of fluid flows, synthetic blood vessels of varying sizes that accommodate different cell types can be facilely produced in a spatiotemporally controlled manner (Figure S11). Two or more heterotypic therapeutic cells can be organized into different vessel compartments to create multifunctional BMVs catering to different therapeutic needs. The BMV–CSC patch technology represents a versatile platform for designing and developing vascularized tissue-engineered constructs for the repair and regeneration of ischemic tissues. The striking functional benefits and the fast and facile fabrication of BMV–CSC patch make it promising for a broad range of applications in tissue engineering and regenerative medicine.

Supplementary Material

Refer to Web version on PubMed Central for supplementary material.

ACKNOWLEDGMENTS

This work was supported by the grants from the National Institutes of Health (R01 HL123920 and HL137093 to K.C.), North Carolina State University Chancellor’s Innovation Fund (to K.C.), and UNC General Assembly Research Opportunities Initiative award (to K.C. and F.L.). We would like to acknowledge Dr. Eva Johannes and the Cellular and Molecular Imaging Facility (CMIF) at North Carolina State University for their assistance. This work was performed in part at the Analytical Instrumentation Facility (AIF) at North Carolina State University, which is supported by the State of North Carolina and the National Science Foundation (award number ECCS-1542015). The AIF is a member of the North Carolina Research Triangle Nanotechnology Network (RTNN), a site in the National Nanotechnology Coordinated Infrastructure (NNCI).

REFERENCES

(1). Prabhu SD; Frangogiannis NG The Biological Basis for Cardiac Repair After Myocardial Infarction. Circ. Res 2016, 119, 91112.

(2). Ziaeian B; Fonarow GC Epidemiology and Aetiology of Heart Failure. Nat. Rev. Cardiol 2016, 13, 368–378. [PubMed: 26935038]

(3). Sun X; Altalhi W; Nunes SS Vascularization Strategies of Engineered Tissues and Their Application in Cardiac Regeneration. Adv. Drug Delivery Rev 2016, 96, 183–194.

(4). Bolli R; Ghafghazi S Stem cells: Cell therapy for cardiac repair: what is needed to move forward? Nat. Rev. Cardiol 2017,14, 257–258. [PubMed: 28361979]

(5). Annabi N; Tsang K; Mithieux SM; Nikkhah M; Ameri A; Khademhosseini A; Weiss AS Highly Elastic Micropatterned Hydrogel for Engineering Functional Cardiac Tissue. Adv. Funct. Mater 2013, 23, 4950–4959.

(6). Tang J; Vandergriff A; Wang Z; Hensley MT; Cores J; Allen TA; Dinh P-U; Zhang J; Caranasos TG; Cheng K A Regenerative Cardiac Patch Formed by Spray Painting of Biomaterials Onto the Heart. Tissue Eng. Part C 2017, 23, 146–155.

(7). Ogle BM; Bursac N; Domian I; Huang NF; Menasché P; Murry CE; Pruitt B; Radisic M; Wu JC; Wu SM; Zhang J; Zimmermann W-H; Vunjak-Novakovic G Distilling Complexity to Advance Cardiac Tissue Engineering. Sci. Transl. Med 2016, 8, 342ps13.

(8). Riemenschneider SB; Mattia DJ; Wendel JS; Schaefer JA; Ye L; Guzman PA; Tranquillo RT Inosculation and Perfusion of Pre-vascularized Tissue Patches Containing Aligned Human Microvessels After Myocardial Infarction. Biomaterials 2016, 97, 51–61. [PubMed: 27162074]

(9). Takebe T; Sekine K; Enomura M; Koike H; Kimura M; Ogaeri T; Zhang R-R; Ueno Y; Zheng Y-W; Koike N; Aoyama S; Adachi Y; Taniguchi H Vascularized and Functional Human Liver fromAniPSC-Derived Organ Bud Transplant. Nature 2013, 499,481–484. [PubMed: 23823721]

(10). Laschke MW; Menger MD Adipose Tissue-Derived Microvascular Fragments: Natural Vascularization Units for Regenerative Medicine. Trends Biotechnol 2015, 33, 442–448. [PubMed: 26137863]

(11). Hasan A; Paul A; Vrana NE; Zhao X; Memic A; Hwang Y-S; Dokmeci MR; Khademhosseini A Microfluidic Techniques for Development of 3D Vascularized Tissue. Biomaterials 2014, 35, 7308–7325. [PubMed: 24906345]

(12). Daniele MA; North SH; Naciri J; Howell PB; Foulger SH; Ligler FS; Adams AA Rapid and Continuous Hydrodynamically Controlled Fabrication of Biohybrid Microfibers. Adv. Funct. Mater 2013, 23, 698–704.

(13). Daniele MA; Adams AA; Naciri J; North SH; Ligler FS Interpenetrating networks based on gelatin methacrylamide and PEG formed using concurrent thiol click chemistries for hydrogel tissue engineering scaffolds. Biomaterials 2014, 35, 1845–1856. [PubMed: 24314597]

(14). DiVito KA; Daniele MA; Roberts SA; Ligler FS; Adams AA Microfabricated Blood Vessels Undergo Neoangiogenesis. Biomaterials 2017, 138, 142–152. [PubMed: 28570946]

(15). Tang J; Shen D; Caranasos TG; Wang Z; Vandergriff AC; Allen TA; Hensley MT; Dinh P-U; Cores J; Li T-S; Zhang J; Kan Q; Cheng K Therapeutic Microparticles Functionalized with Biomimetic Cardiac Stem Cell Membranes and Secretome. Nat. Commun 2017, 8, 13724. [PubMed: 28045024]

(16). Tang J; Cui X; Caranasos TG; Hensley MT; Vandergriff AC; Hartanto Y; Shen D; Zhang H; Zhang J; Cheng K Heart Repair Using Nanogel-Encapsulated Human Cardiac Stem Cells in Mice and Pigs with Myocardial Infarction. ACS *Nano* 2017, 11, 9738–9749. [PubMed: 28929735]

(17). Weinberg C; Bell E A Blood Vessel Model Constructed from Collagen and Cultured Vascular Cells. Science 1986, 231, 397–400. [PubMed: 2934816]

(18). Gui L; Dash BC; Luo J; Qin L; Zhao L; Yamamoto K; Hashimoto T; Wu H; Dardik A; Tellides G; Niklason LE; Qyang Y Implantable Tissue-Engineered Blood Vessels From Human Induced Pluripotent Stem Cells. Biomaterials 2016, 102, 120–129. [PubMed: 27336184]

(19). Daniele MA; Radom K; Ligler FS; Adams AA Microfluidic Fabrication of Multiaxial Microvessels via Hydrodynamic Shaping. RSC Adv. 2014, 4, 23440–23446.

(20). Marieb EN; Hoehn K Human Anatomy and Physiology, 8th ed.; Benjamin Cummings: San Francisco, CA, 2010, p 698.

(21). Broaddus VC; Mason RC; Ernst JD; King TE; Lazarus SC; Murray JF; Nadel JA; Slutsky AS; Gotway MB Murray and Nadels Textbook of Respiratory Medicine, 6th ed.; Elsevier Saunders: Philadelphia, PA, 2016, p 10.

(22). Paulsson MM Basement Membrane Proteins: Structure, Assembly, and Cellular Interactions. Crit. Rev. Biochem. Mol. Biol 1992, 27, 93–127. [PubMed: 1309319]

(23). Huang NF; Okogbaa J; Lee JC; Jha A; Zaitseva TS; Paukshto MV; Sun JS; Punjya N; Fuller GG; Cooke JP The Modulation of Endothelial Cell Morphology, Function, and Survival Using Anisotropic Nanofibrillar Collagen Scaffolds. Biomaterials 2013, 34, 4038–4047. [PubMed: 23480958]

(24). Knowles TPJ; Buehler MJ Nanomechanics of Functional and Pathological Amyloid Materials. Nat. Nanotechnol 2011, 6, 469–479. [PubMed: 21804553]

(25). Liu T; Houle JD; Xu J; Chan BP; Chew SY Nanofibrous Collagen Nerve Conduits for Spinal Cord Repair. Tissue Eng., Part A 2012, 18, 1057–1066. [PubMed: 22220714]

(26). Wang X; Salick MR; Wang X; Cordie T; Han W; Peng Y; Li Q; Turng L-S Poly(*ε*-caprolactone) Nanofibers with a Self-Induced Nanohybrid Shish-Kebab Structure Mimicking Collagen Fibrils. Biomacromolecules 2013, 14, 3557–3569. [PubMed: 24010580]

(27). Jeon O; Ryu SH; Chung JH Control of Basic Fibroblast Growth Factor Release from Fibrin Gel with Heparin and Concentrations of Fibrinogen and Thrombin. J. Controlled Release 2005, 105, 249–259.

(28). Qian L; Shim W; Gu Y; Shirhan M; Lim KP; Tan LP; Lim CH; Sin YK; Wong P Hemodynamic Contribution of Stem Cell Scaffolding in Acute Injured Myocardium. Tissue Eng., Part A 2012, 18, 1652–1663. [PubMed: 22607369]

(29). Gómez-Gaviro MV; Lovell-Badge R; Fernández-Aviles F; Lara-Pezzi E The Vascular Stem Cell Niche. J. Cardiovasc. Transl. Res 2012, 5, 618–630. [PubMed: 22644724]

(30). Bautch VL Stem Cells and The Vasculature. Nat. Med 2011, 17, 1437–1443. [PubMed: 22064433]

(31). Aguirre A; Planell JA; Engel E Dynamics of Bone Marrow-Derived Endothelial Progenitor Cell/Mesenchymal Stem Cell Interaction in Co-Culture and Its Implications in Angiogenesis. Biochem. Biophys. Res. Commun 2010, 400, 284–291. [PubMed: 20732306]

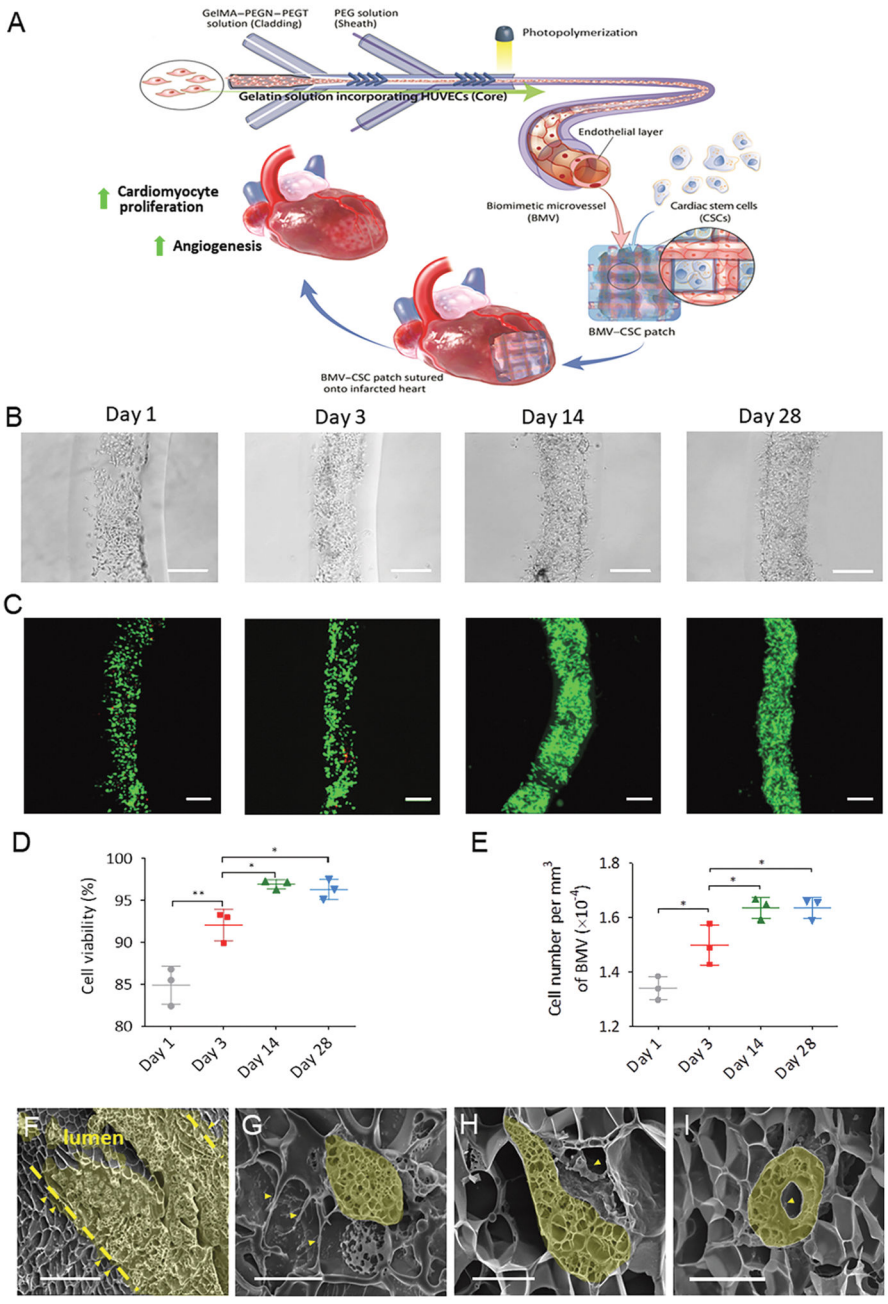

Figure 1.

(A) Schematic illustration of the fabrication process of the BMV–CSC patch. The therapeutic potential of the BMV–CSC patch is tested in a rat model of acute MI. (B) Bright-field images showing the attachment and growth of HUVECs on the luminal surface of BMV during 28 days of culture. (C) LIVE/DEAD staining of the HUVECs in BMV after being cultured for 1, 3, 14, and 28 days. Green: live cells, red: dead cells. (D) Cell viability of the HUVECs at different time intervals. (E) Number of HUVECs per mm^3 after being cultured in BMV for 1, 3, 14, and 28 days. $n = 3$ for each time point. (F–I) Scanning electron microscopy (SEM) reveals the morphology of HUVECs in the lumen of BMV at day 14. The dashed lines denote the boundaries of the lumen (F). The maturation ofHUVECs in

BMV was detected, indicating the formation ofpseudopodia (G), protrusions (H), and a capillary-like hollow structure (I) extending into the BMV matrix. Scale bars, 250 μ*m* (B,C); 50 μ*m* (F); 10 μ*m* (G–I). The data in (D,E) are plotted on an expanded scale. The cross sections of the representative cells in (F–I) were highlighted in yellow. All data are mean ± SD. * indicates $p < 0.05$, ** indicates $p < 0.01$. Comparisons among more than two groups were performed using one-way ANOVA, followed by post hoc Bonferroni test.

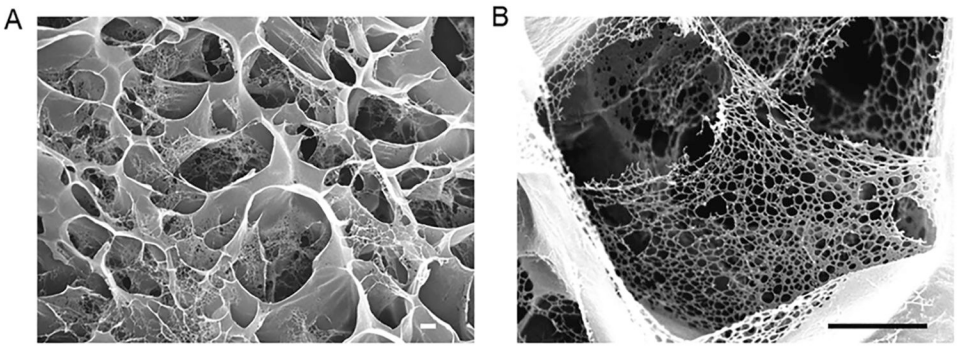

Figure 2.

(A) SEM image of noncellularized BMV. (B) High magnification of the BMV, showing the nanofibrous architecture of its pore walls. Scale bars, 1 μm.

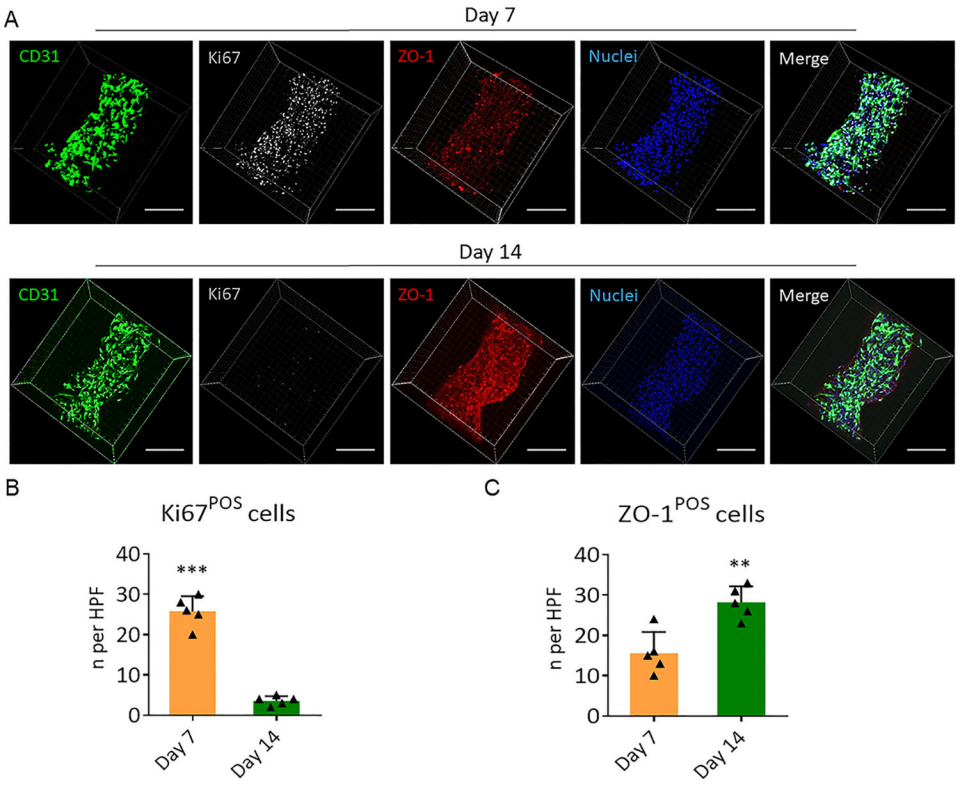

Figure 3.

(A) Expression of the endothelial-specific marker, CD31 (green), proliferation marker, Ki67 (gray), and tight junction protein, ZO-1 (red), in the HUVECs in BMVs. Nuclei were stained with DAPI (blue). Scale bars, 250 μm. (B,C) Quantitative analysis of Ki67-positive and ZO-1-positive HUVECs after being cultured for 7 and 14 days, respectively. The numbers of Ki67-positive or ZO-1-positive cells in five high-power microscopic fields (×40 objective) were averaged. All data are mean ± SD. Comparisons between any two groups were performed using two-tailed unpaired Student's *t*-test. ** indicates $p < 0.01$, *** indicates $p < 0.001$.

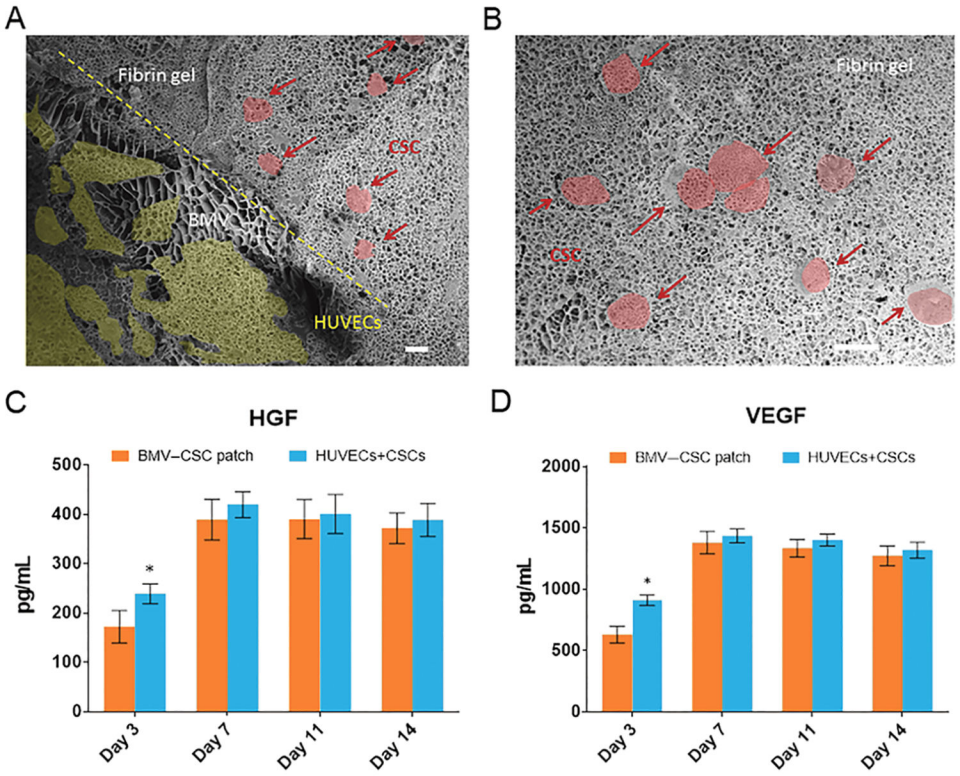

Figure 4.

(A,B) Microstructure of the BMV–CSC patch containing BMVs (A) and human CSCs (B) after 22 days of in vitro culture. Scale bars, 10 ***μ***m. The HUVECs in BMV and CSCs were highlighted in yellow and red, respectively. (C,D) Release of paracrine factors, namely, HGF and VEGF, in the conditioned media of the BMV–CSC patch and the coculture of HUVECs and CSCs with equivalent cell number in the patch on standard TCP (***n*** = 3 for each group at each time point). All data are mean ± SD. Comparisons between any two groups were performed using two-tailed unpaired Student's ***t***-test. * indicates ***p*** < 0.05 when compared with the BMV–CSC patch.

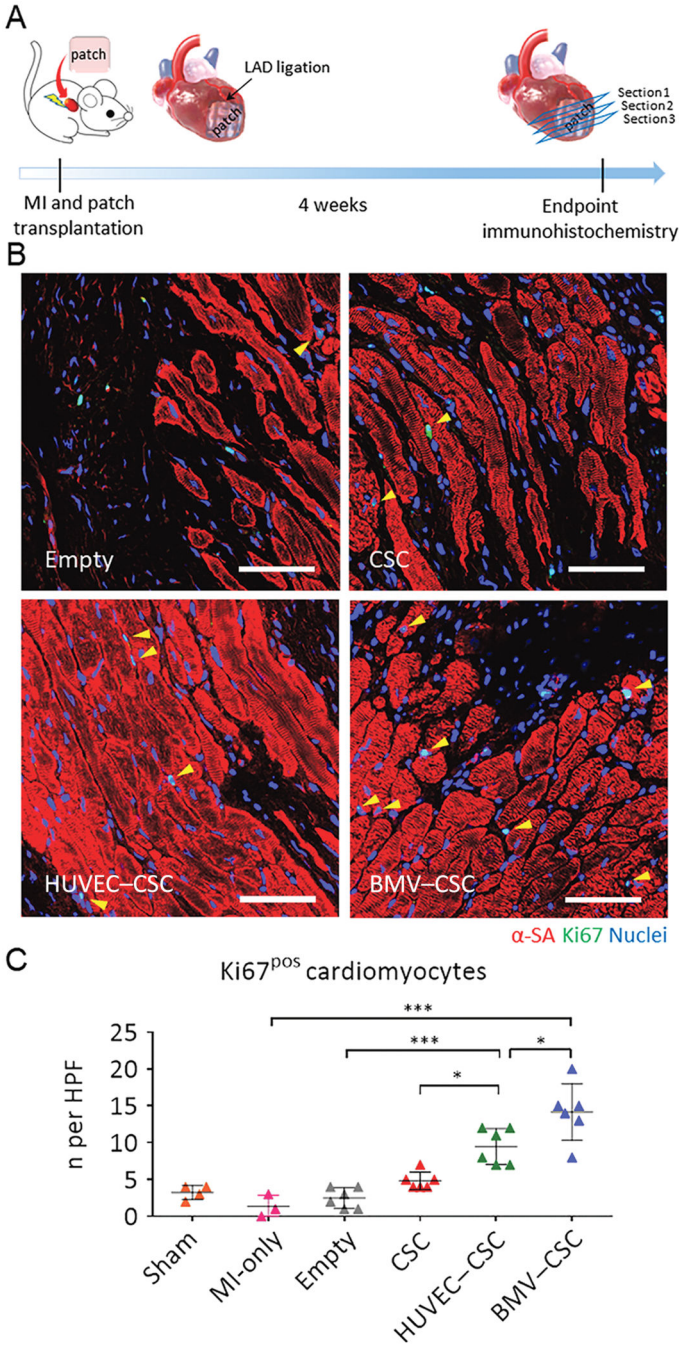

Figure 5.

(A) Schematic illustration of the animal study design. (B) Representative images showing cycling cardiomyocytes (yellow arrowheads) as indicated by ***α***-SA and Ki67 double-positive cardiomyocytes in the peri-infarct regions of empty patch-, CSC patch-, HUVEC–CSC patch-, and BMV–CSC patch-treated hearts at week 4. (C) Quantification of Ki67-positive cardiomyocytes at week 4 in the sham (***n*** =4), MI-only (***n*** = 3), emptypatch (***n*** = 6), CSC patch (***n*** = 6), HUVEC–CSC patch (***n*** = 6), and BMV–CSC patch (***n*** = 6) groups. Scale bars,

50 μm. All data are mean ± SD. * indicates $p < 0.05$; ** indicates $p < 0.01$; *** indicates $p < 0.001$.

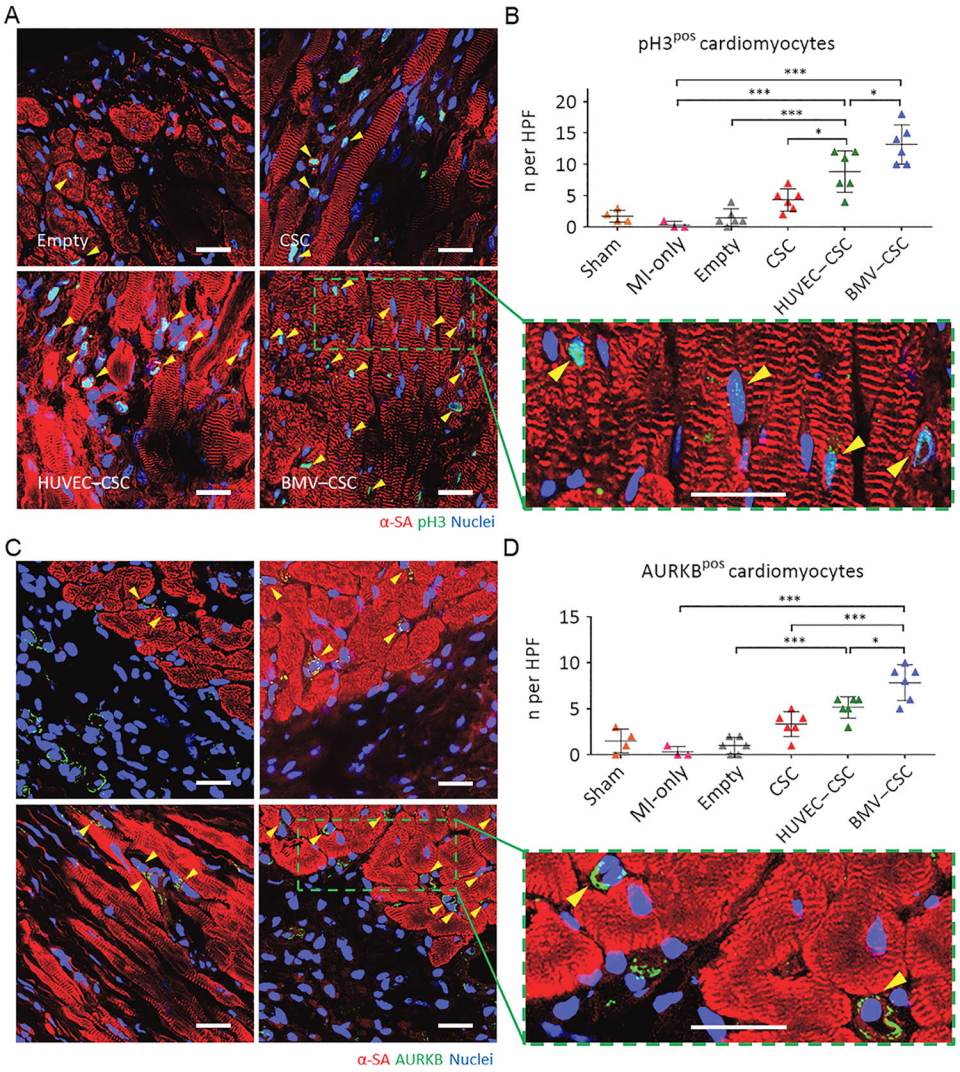

Figure 6.

(A,B) Visualization of phospho-histone H3 phosphorylation in cardiomyocytes (yellow arrowheads) in the peri-infarct regions of empty patch-, CSC patch-, HUVEC–CSC patch-, and BMV–CSC patch-treated hearts at week 4. Representative images are in (A) (blue: DAPI, staining nuclei; red: α-sarcomeric actinin, staining cardiomyocytes; green: pH3, indicating the cells that are in late G2/mitosis phase; the green square highlights the localization of pH3 (yellow arrowheads) in the nuclei of cycling cardiomyocytes). Quantification in (B) shows pH3-positive cardiomyocytes at week4 in the sham (n =4), MI-only (n = 3), emptypatch (n = 6), CSC patch (n = 6), HUVEC–CSC patch (n = 6), and BMV–CSC patch (n = 6) groups. (C,D) Visualization of AURKB in cardiomyocytes (yellowarrowheads) in the peri-infarct regions of emptypatch-, CSC patch-, HUVEC–CSC patch-, and BMV–CSC patch-treated hearts at week 4. Representative images are in (C) (blue: DAPI, staining nuclei; red: α-sarcomeric actinin, staining cardiomyocytes; green: AURKB, marking the cells in karyokinesis and cytokinesis; the green square highlights the localization of AURKB in midbodies (yellow arrowheads). Quantification in (D) shows AURKB-positive cardiomyocytes at week 4 in the sham (n = 4), MI-only (n = 3), empty

patch ($n = 6$), CSC patch ($n = 6$), HUVEC–CSC patch ($n = 6$), and BMV–CSC patch ($n = 6$) groups. Scale bars, 20 μm. All data are mean ± SD. * indicates $p < 0.05$; ** indicates $p < 0.01$; *** indicates $p < 0.001$.

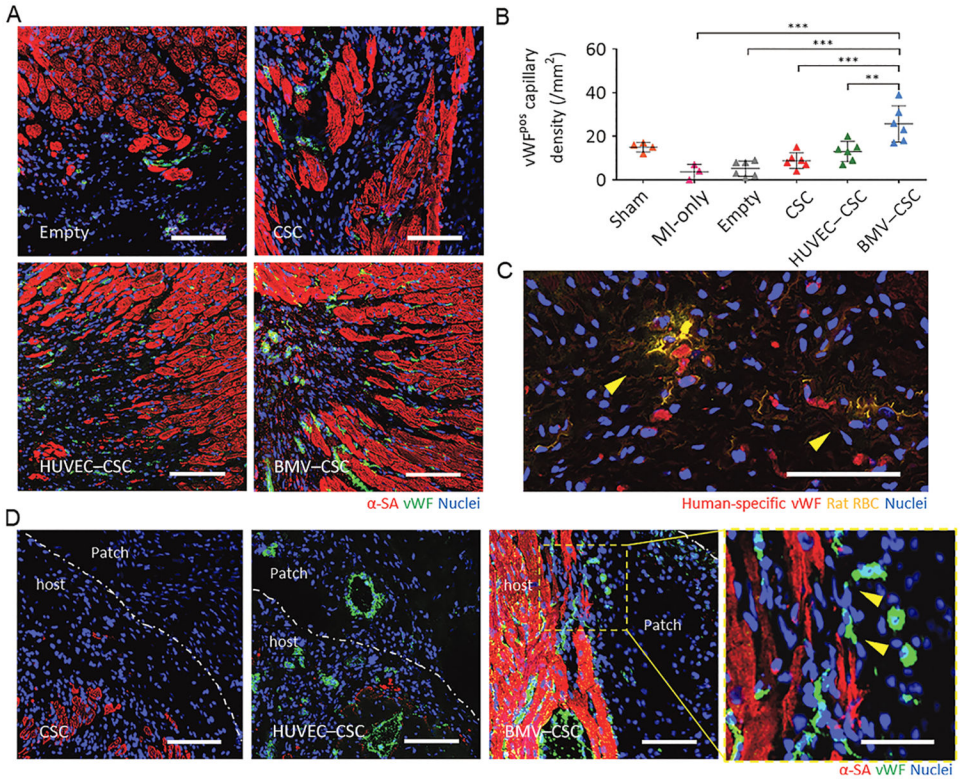

Figure 7.

(A) Representative images showing vWF-positive vascular structures in the peri-infarct regions of emptypatch-, CSC patch-, HUVEC–CSC patch-, and BMV–CSC patch-treated hearts at week 4. (B) Quantification of the vWF-positive capillary densityatweek4in the sham (***n*** = 4), MI-only (***n*** = 3), empty patch (***n*** = 6), CSC patch (***n*** = 6), HUVEC–CSC patch (***n*** = 6), and BMV–CSC patch (***n*** = 6) groups. (C) Rat RBC stain (yellow) showing the RBCs in perfused vWF-positive human vessels (red) in the peri-infarct region of BMV–CSC patch-treated hearts at week 4. (D) Representative images showing neovascularization at the host–patch interface in the hearts treated with different patches at week 4. The yellow square highlights vWF-positive vasculatures (yellow arrowheads) undergoing anastomosis at the host–patch interface of the BMV–CSC patch-treated heart. Scale bars, 100 ***μ***m, except for those in (C) and the yellows quare in (D), which are 50 ***μ***m, respectively. ** indicates $p < 0.01$; *** indicates $p < 0.001$.